Published in: Experimental Eye Research (2009)
Status: Postprint (Author's version)

Additional parameters for the morphometry of angiogenesis and lymphangiogenesis in corneal flat mounts

S. Blacher, B. Detry, F. Bruyère, J.-M. Foidart, A. Noël
Laboratory of Tumor and Development Biology, Groupe Interdisciplinaire de Gênomique Appliquée-Cancer (GIGA-Cancer), University of Liège, Tour de Pathologie (B23), B-4000 Sart-Tilman, Belgium

Recently, Bock et al. (2008) proposed a semiautomatic method to quantify the angiogenesis and the lymphangiogenesis in corneal flat mounts. This model has proven suitability for unraveling the cellular and molecular mechanisms of inflammatory corneal lymphangiogenesis, as well as for evaluating the efficacy of novel drugs (Bock et al., 2007). The new method proposed by Bock et al. (2008) follows the classical steps of image analysis, i.e., image pre-processing in order to eliminate noise and enhance the contrast between the vessels and the background and then, a threshold transformation by which pixels belonging to vessels take the value of 1 (white pixels) and pixels for the background are scored 0 (black pixels). Once such a binary image is generated, Bock et al. (2008) measure automatically the area of the neovascularisation. This elegant methodology represents a great improvement as compared to the manual methods usually used to quantify the (lymph)angiogenic response observed in such murine model.

The purpose of this letter is to show that additional morpho-metric parameters can be determinated from the binary processed image of the cornea leading to a more detailed characterisation of the corneal structure. Indeed, the vascularized area as determined by Bock et al. (2008) is a global measurement which enables an accurate determination of an increase/decrease of the vascularisation in the whole cornea, for example, as a function of time or when the cornea is submitted to pharmacological treatment. However, as it is a global measurement, it does not give insights into morphological changes of the vascular structure putatively induced by the treatment. Based on our expertise gained on image analysis of (lymph)angiogenesis in various experimental models (Blacher et al., 2001, 2005, 2008; Bruyere et al., 2008), we propose, in addition to the determination of area vascular density, to complete the description of the vascular tree of the cornea by measuring the five following parameters: (1) the total length density (δ_L) of vessel structure, which is a complementary measurement to the vessel area density (δ_A), (2) the density of vessel extremities (δ_V) which quantifies the increase/decrease of the number of new vessels, (3) the density of nodes (δ_n) (including branching and overlapping vessels) which characterizes the complexity of the structure, (4) the vessel density distribution which determines the spatial allocation of vessels, and (5) the maximal length of migration of vessels (L_{max}).

The pre-processing of images was performed as proposed by these authors with minor modifications due to the particular image acquisition conditions (microscope, camera...). Image analysis and statistics were performed using the Matlab software 7.1. A typical grey level image of the cornea and the corresponding thresholded image are shown in Fig. la and b, respectively. It is worth noting that physiological limbal vessels were erased manually in the binary image. From the thresholded image of vessels (Fig. lb), the total area of the vascular tree was determined automatically, as described by Bock et al. (2008). This value was divided by the total area of the cornea to obtain δ_A. The total length density (δ_L), the vessel extremities (δ_V) and nodes' (δ_n) densities were determined as described (Blacher et al., 2005). The skeleton of the vessel tree as well as the vessel extremities and nodes, obtained from the thresholded image (Fig. lb) are presented in Fig. 1c and d, respectively. It must be remarked that in Fig. lc, spurious vessels' extremities generated from removal limbic vessels, were eliminated. Image transformations used to measure the vessel density distribution and L_{max} are described in Fig. le and f.

In order to validate the proposed approach, it has been applied on whole mounts of cornea issued from mice treated or not with Ro-28-2653, an inhibitor of matrix metalloproteases (MMPs). Ro-28-2653 is a potent MMP inhibitor with high selectivity for MMP2, MMP9 and MT1-MMP (MMP14) (Maquoi et al., 2004) whose functions in pathological angiogenesis are well documented (Bergers et al., 2000; Hiraoka et al.,1998; Itoh et al., 1998; Kato et al., 2001; Masson et al., 2005; Noel et al., 2008). Notably, MMP2 and MMP9 have been also implicated in choroidal angiogenesis (Lambert et al., 2003; Noel et al., 2007). In addition, the implication of these MMPs during lymphangiogenesis has emerged recently (Bruyere et al., 2008; Rutkowski et al., 2006).

Mice of C57B16 background were intra-peritonealy injected, once a day during 9 days, with vehicle or RO-28-2653 (30 mg/kg) prepared as previously described (Maquoi et al., 2004). Corneal lymphangiogenesis was induced by thermal cauterization of the central cornea with an ophthalmic cautery (OPTEMP II V, Alcon Surgical, Fort Worth, USA) two days after the first injection of MMP inhibitor. Typical grey level images of the

control and RO-28-2653-treated cornea as well as the spatial density vessel distribution are presented in Fig. lg-i, respectively. The measured densities δ_A, δ_L, δ_V, and δ_b, and L_{max} are presented in Table 1.

Global analysis of the vasculature as determined by the vessel area density (δ_A) and the total length density (δ_L) reveals that vessel growth was significantly inhibited by RO-28-2653. Furthermore, the decrease of the density of vessel extremities (δ_V) indicates that RO-28-2653 also blocked the sprouting of new vessels. Accordingly, the decrease of the density of nodes (δ_n) points out a less complex vascular structure. Such response is further confirmed by the wider spatial density vessel distribution for the control (see vessel density distribution in Fig. 1i). It is worth noting that the maximal length of migration is not significantly different between the control and RO-28-2653-treated animals. This data with the decreased value of δ_b and δ_V reveal that RO-28-2653 inhibited the sprouting of new vessels but not the rate of large vessel migration.

Altogether these data clearly demonstrate that the proposed methodology is suitable to pinpoint and quantify both global and local morphometric differences in the vascular network. Of major interest is the fact that this technique could detect any local morphologic changes of the lymphatic networks whereas the global density is unchanged, and *vice versa.* We therefore recommend completing the method reported by Bock et al. (2008) by evaluating the additional parameters described here to get information on the different steps of the lymphangiogenesis process (activation, proliferation and migration of endothelial cells).

Table 1

*Statistical parameters for the vessel area density (δ_A), the area the total length density (δ_L), the density of vessel extremities (δ_V), the density of nodes (δ_n) as well as for the maximal length of migration of vessels (L_{max}). ** indicates $p < 0.01$ in Wilcoxon test. N = 5.*

	δ_A**	δ_L(l/mm^2)**	δ_V (l/mm^2)	δ_b (l/mm^2)	L_{max} (mm)
Control	0.1695 ± 0.0122	95.19 ± 3.89	42.31 ± 4.38	54.12 ± 3.97	0.98 ± 0.10
RO-28-2653	0.1102 ± 0.0102	62.83 ± 5.37	26.02 ± 2.47	36.52 ± 4.09	0.95 ± 0.08

Fig. 1. *Lymphangiogenesis has been induced by corneal cauterization,* (a) Typical image obtained in the corneal lymphangiogenesis assay, (b) corresponding thresholded image. Threshold was determined automatically using the entropy of histogram of grey level intensities (Kapur et al., 1985). (c) Vessel extremities and (d) node points are superposed (in green) to the skeleton of the vascular tree (in red). Parametric pruning transformation was applied to eliminate spurious branches (Soille, 1999). (e) Euclidean distance of the smallest polygon containing the cornea vascular tree. By this transformation, it is assigned to each pixel of the polygon a grey level intensity corresponding to the distance between that pixel and the nearest external border of the polygon. It is seen that pixels near the border of the polygon are dark (short distances) and lighten toward the centre of the cornea (high distances), (f) Allocation to each vasculature pixels of an intensity corresponding to the distance to the limit of the structure. Binary image of vessels (Fig. 1b) was multiplied (pixel by pixel) by the Euclidean distance of the polygon image (Fig. 1e). These results in a grey level image (Fig. 1f) in which each pixel which belongs to the vasculature takes an intensity corresponding to the distance to the limit of the cornea and the remainder pixels take intensity equal to 0. Statistical analysis of pixel intensities leads to the mean spatial distribution of each pixel belonging to the vessels as a function to the nearest border of the vascular tree. Typical grey level images of the control (g) and of the RO-28-2653-treated cornea (h) and the corresponding spatial density vessel distribution (i). ** indicates $p < 0.01$ in the Wilcoxon test. (For interpretation of the references to colour in this figure legend, the reader is referred to the web version of this article.)

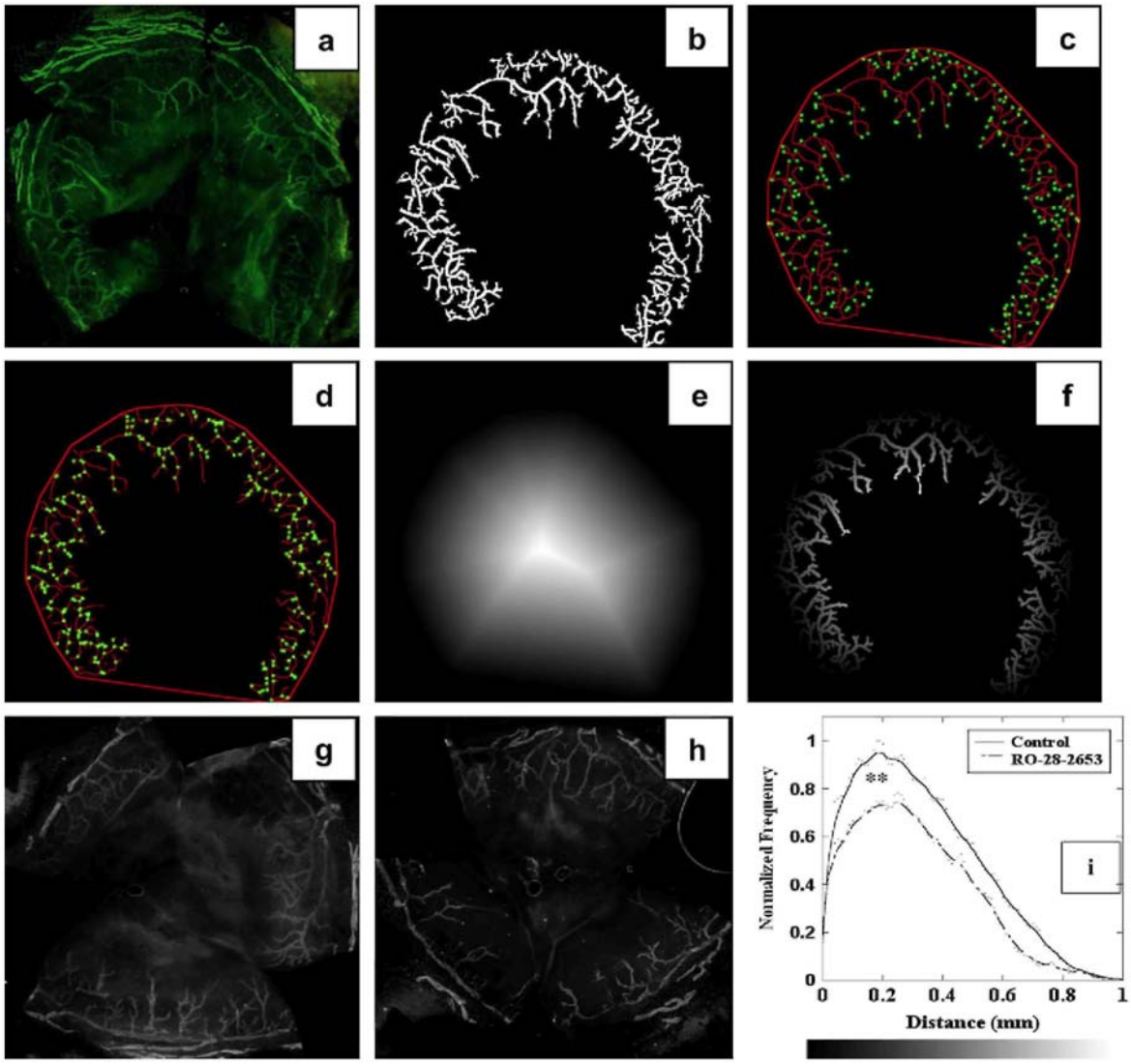

Acknowledgements

This work was supported by grants from the FP7-HEALTH-2007-A (No. 201279) "MICROENVIMET" and the Program No. 616476 "NEANGIO" from the "Région Wallonne".

References

Bergers, G., Brekken, R., McMahon, G., Vu, T.H., Itoh, T., Tamaki, K., Tanzawa, K., Thorpe, P., Itohara, S., Werb, Z., Hanahan, D., 2000. Matrix metalloproteinase-9 triggers the angiogenic switch during carcinogenesis. Nat. Cell. Biol. 2, 737-744.

Blacher, S., Devy, L, Burbridge, M.F., Roland, G., Tucker, G., Noel, A., Foidart, J.M., 2001. Improved quantification of angiogenesis in the rat aortic ring assay. Angiogenesis 4,133-142.

Blacher, S., Devy, L., Hlushchuk, R, Larger, E., Lamandé, N., Burri, P., Corvol, P., Djonov, V.G., Foidart, J.M., Noel, A., 2005. Quantification of angiogenesis in the chicken chorioallantoic membrane (CAM). Image Anal. Stereol. 24,169-180.

Blacher, S., Jost, M., Melen-Lamalle, L, Lund, L.R., Romer, J., Foidart, J.M., Noel, A., 2008. Quantification of in vivo tumor invasion and vascularization by computerized image analysis. Microvasc. Res. 75,169-178.

Bock, F, Onderka, J., Dietrich, T, Bachmann, B., Kruse, F.E., Paschke, M., Zahn, G., Cursiefen, C, 2007. Bevacizumab as a potent inhibitor of inflammatory corneal angiogenesis and lymphangiogenesis. Ophthalmol. Vis. Sci. 48, 2545-2552.

Bock, F, Onderka, J., Hos, D., Horn, F, Martus, P., Cursiefen, C, 2008. Improved semiautomatic method for morphometry of angiogenesis and lymphangiogenesis in corneal flatmounts. Exp. Eye Res. 87 (5), 462-470.

Bruyere, F, Melen-Lamalle, L, Blacher, S., Roland, G., Thiry, M., Moons, L, Frankenne, F, Carmeliet, P., Alitalo, K., Libert, C, Sleeman, J.P., Foidart, J.M., Noel, A., 2008. Modeling lymphangiogenesis in a three-dimensional culture system. Nat. Methods 5, 431-437.

Hiraoka, N., Allen, E., Apel, I.J., Gyetko, M.R., Weiss, S.J., 1998. Matrix metal-loproteinases regulate neovascularization by acting as pericellular fibrinolysins. Cell 95, 365-377.

Itoh, T., Tanioka, M., Yoshida, H., Yoshioka, T, Nishimoto, H., Itohara, S., 1998. Reduced angiogenesis and tumor progression in gelatinase A-deficient mice. Cancer Res. 58,1048-1051.

Kapur, J.N., Sahoo, P.K., Wong, A.K.C., 1985. A new method for gray-level picture thresholding using the entropy of the histogram. Comput. Vision Graph. Image Process. 29, 273-285.

Kato, T., Kure, T, Chang, J.H., Gabison, E.E., Itoh, T, Itohara, S., Azar, D.T., 2001. Diminished corneal angiogenesis in gelatinase A-deficient mice. FEBS Lett. 508, 187-190.

Lambert, V., Wielockx, B., Munaut, C, Galopin, C, Jost, M., Itoh, T, Werb, Z., Baker, A., Libert, C, Krell, H.W, Foidart, J.M., Noel, A., Rakic, J.M., 2003. MMP-2 and MMP-9 synergize in promoting choroidal neovascularization. FASEB J. 17, 2290-2292.

Maquoi, E., Sounni, N.E., Devy, L, Olivier, F, Frankenne, F, Krell, H.W, Grams, F, Foidart, J.M., Noel, A., 2004. Anti-invasive, antitumoral, and antiangiogenic efficacy of a pyrimidine-2,4,6-trione derivative, an orally active and selective matrix metalloproteinases inhibitor. Clin. Cancer Res. 10, 4038-4047.

Masson, V., de la Ballina, L.R., Munaut, C, Wielockx, B., Jost, M., Maillard, C, Blacher, S., Bajou, K., Itoh, T, Itohara, S., Werb, Z., Libert, C, Foidart, J.M., Noel, A., 2005. Contribution of host MMP-2 and MMP-9 to promote tumor vascularization and invasion of malignant keratinocytes. FASEB J. 19, 234-236.

Noel, A., Jost, M., Lambert, V., Lecomte, J., Rakic, J.M., 2007. Anti-angiogenic therapy of exudative age-related macular degeneration: current progress and emerging concepts. Trends Mol. Med. 13, 345-352.

Noel, A., Jost, M., Maquoi, E., 2008. Matrix metalloproteinases at cancer tumor-host interface. Semin. Cell Dev. Biol. 19, 52-60.

Rutkowski, J.M., Boardman, K.C., Swartz, M.A., 2006. Characterization of lymphangiogenesis in a model of adult skin regeneration. Am. J. Physiol. Heart Circ. Physiol. 291, H1402-1410.

Soille, P., 1999. Morphological image analysis. Springer-Verlag, Berlin, Heidelberg, New York.